Mechanics of Advanced Materials and Structures

ISSN: 1537-6494 (Print) 1537-6532 (Online) Journal homepage: http://www.tandfonline.com/loi/umcm20

An enriched macro finite element for the static analysis of thick general quadrilateral laminated composite plates

Rita F. Rango, Liz G. Nallim & Sergio Oller

To cite this article: Rita F. Rango, Liz G. Nallim & Sergio Oller (2016) An enriched macro finite element for the static analysis of thick general quadrilateral laminated composite plates, Mechanics of Advanced Materials and Structures, 23:10, 1197-1206, DOI: 10.1080/15376494.2015.1068400

To link to this article: http://dx.doi.org/10.1080/15376494.2015.1068400

Accepted author version posted online: 15 Jul 2015.
Published online: 23 Mar 2016.

MECHANICS OF ADVANCED MATERIALS AND STRUCTURES
2016, VOL. 23, NO. 10, 1197–1206
http://dx.doi.org/10.1080/15376494.2015.1068400

Taylor & Francis
Taylor & Francis Group

ORIGINAL ARTICLE

An enriched macro finite element for the static analysis of thick general quadrilateral laminated composite plates

Rita F. Rango[a], Liz G. Nallim[a], and Sergio Oller[b,c]

[a]Facultad de Ingeniería, INIQUI (CONICET), Universidad Nacional de Salta, Salta, Argentina; [b]CIMNE International Center for Numerical Method Engineering, Barcelona, Spain; [c]UPC, Technical University of Catalonia (Barcelona Tech), Barcelona, Spain

ABSTRACT
This article presents the formulation of an enriched macro finite element based on the trigonometric shear deformation theory for the static analysis of symmetrically laminated composite plates. Shear correction factor is not required because this theory accounts for tangential stress-free boundary conditions on the plate boundary surfaces. The macro element is obtained using the principle of virtual work and Gram-Schmidt orthogonal polynomials as enrichment functions. The implementation of the obtained algorithm is simple and efficient, and allows studying general quadrilateral plates with a single macro element. Several examples are presented to show the capability and applicability of the developed formulation.

ARTICLE HISTORY
Received 25 November 2014
Accepted 5 April 2015

KEYWORDS
Laminated composite plates; macro finite element; static analysis; trigonometric shear deformation theory; general quadrilateral plates

1. Introduction

Composite materials are mainly preferred in aerospace, marine, and automobile engineering because of their advanced properties and tailoring capability, and have the potential for incorporating optimum design techniques into the design process of candidate structures.

For the efficient employment of laminated plates it is necessary to use the appropriated theories and methodologies to predict accurately their structural behavior. In this sense the use of three-dimensional (3D) elasticity theory leads to a more accurate determination of transverse shear stresses. However, the employment of 3D elasticity theory increases significantly the computational cost. For this reason many equivalent single layers (ESL) plate theories [1] have been proposed to reduce the 3D problems to the 2D ones. The simplest ESL theory is the classical laminated plate theory (CLPT), which is based on Kirchhoff's hypothesis and provides reasonable results for thin plates [2]. The first-order shear deformation theory (FSDT), based on the works of Reissner [3] and Mindlin [4], assumes constant transverse shear stresses and therefore it requires the use of a shear correction factor, which may be difficult to compute because this factor varies with the loading conditions, lamination sequences, and boundary conditions [5].

In order to consider traction-free boundary conditions and transverse shear effects, avoiding the use of shear correction factors, different higher order shear deformation theories (HSDT) have been proposed [6–10].

Among many HSDT, only few higher-order shear deformation theories have been developed containing non-polynomial shape strain functions. In particular, trigonometric shear deformation theories were recently applied to composite plates by Ferreira et al. [11], Xiang et al. [12], Mantari et al. [13], among others. These theories provide continuity of displacements and zero transverse shear stresses at top and bottom surfaces of the laminate, without the burden of extra degrees of freedom as in layer-wise formulations. As stated by Mantari et al. [13], it can be said that there are evidences of the demand of trigonometric shear deformation theories, mainly because they are richer than polynomial functions and the free surface boundary conditions can be guaranteed a priori.

On the other hand, exact solutions for deflections and stresses on arbitrary laminated plate domain, and for general boundary conditions are very difficult, if not impossible, to obtain [1]. The methods for solving the governing equations include different approaches, such as the finite element method [14–17], the finite volume method [18], or the finite difference method [19], which require mesh generations. Other methodologies called meshless methods have been developed [20]. An interesting review focusing mainly on the developments of element-free or meshless methods and their applications in the analysis of composite structures has been reported by Liew et al. [21].

A hierarchical version of finite element method (FEM) in conjunction with the trigonometric shear deformation theory has been proposed for Rango et al. [22] for the free vibration analysis of thick composite laminated plates. Here, this hierarchical version is extended, generalized, and applied for the first time to analyze the static behavior of thick composite laminated plates with general quadrilateral planform and boundary conditions. The macro finite element is formulated using the principle of virtual work and incorporating Gram-Schmidt orthogonal polynomials as enriched functions. Further major benefits of the hierarchical method are the retention of the stiffness coefficients as the order of interpolation is increased [23].

Some numerical examples are used to demonstrate the convergence and accuracy of the proposed methodology in computing global and local responses, which are fundamental to

CONTACT Rita F. Rango ritarango@conicet.gov.ar Facultad de Ingenieria, INIQUI (CONICET), Universidad Nacional de Salta, Av. Bolivia 5150, Salta 4400, Argentina.
Color versions of one or more of the figures in the article can be found online at www.tandfonline.com/umcm.

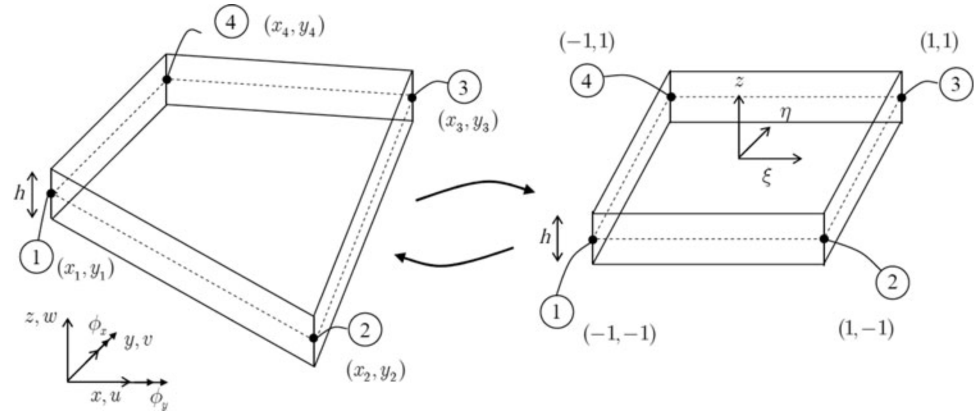

Figure 1. General quadrilateral thick laminated plate cement in Cartesian coordinates (x, y) and natural coordinates (ξ, η).

detect potential areas of starting and propagation of damage. Comparisons with results available in the literature are also presented. After establishing the accuracy of the present formulation, benchmark results for laminated plates with different geometric planform and boundary conditions are presented.

2. Statement of the problem

A general quadrilateral thick laminated plate element is represented based on a four-node scheme, along with Cartesian coordinates (x, y) and natural coordinates (ξ, η) as shown in Figure 1. A symmetric laminate of uniform thickness h with N_l layers is adopted for the analysis.

According to the trigonometric shear deformation theory (TSDT) of plates [11], the in-plane displacement components: u(along the x direction) and v (along the y direction), and the transverse displacement component w (along the z direction) are approximated through the thickness of the plate as:

$$\begin{aligned} u(x, y, z) &= -z\frac{\partial w_0(x, y)}{\partial x} + \sin\frac{\pi z}{h}\phi_x(x, y) \\ v(x, y, z) &= -z\frac{\partial w_0(x, y)}{\partial y} + \sin\frac{\pi z}{h}\phi_y(x, y), \\ w(x, y, z) &= w_0(x, y) \end{aligned} \tag{1}$$

where w_0 is the displacement of a generic point on the midplane $(z = 0)$ and ϕ_x, ϕ_y are the rotation components of the transverse normal about y and x axes, respectively. Employing Eq. (1) and based on the linear elasticity theory, the non-zero strain tensor components at an arbitrary material point of the plate become:

$$\boldsymbol{\varepsilon} = \sin\frac{\pi z}{h}\boldsymbol{\varepsilon}_s - z\boldsymbol{\varepsilon}_\kappa, \quad \boldsymbol{\gamma} = \frac{\pi}{h}\cos\frac{\pi z}{h}\boldsymbol{\varphi}, \tag{2}$$

where

$$\begin{aligned} \boldsymbol{\varepsilon} &= \left\{\varepsilon_{xx} \quad \varepsilon_{yy} \quad \gamma_{xy}\right\}^T \\ \boldsymbol{\varepsilon}_s &= \left\{\frac{\partial \phi_x}{\partial x} \quad \frac{\partial \phi_y}{\partial y} \; \frac{\partial \phi_x}{\partial y} + \frac{\partial \phi_y}{\partial x}\right\}^T \\ \boldsymbol{\varepsilon}_k &= \left\{\frac{\partial^2 w}{\partial x^2} \quad \frac{\partial^2 w}{\partial y^2} \; 2\frac{\partial^2 w}{\partial x \partial y}\right\}^T \\ \boldsymbol{\gamma} &= \left\{\gamma_{yz} \; \gamma_{xz}\right\}^T \quad and\; \boldsymbol{\varphi} = \left\{\phi_y \; \phi_x\right\}^T \end{aligned} \tag{3}$$

The constitutive relations of the kth layer having any fiber orientation in the plane (x, y) can be obtained in the global (x, y, z) coordinate system from:

$$\begin{Bmatrix} \sigma_{xx} \\ \sigma_{yy} \\ \tau_{xy} \\ \tau_{xz} \\ \tau_{yz} \end{Bmatrix}^{(k)} = \begin{bmatrix} \bar{Q}_{11} & \bar{Q}_{12} & \bar{Q}_{16} & 0 & 0 \\ \bar{Q}_{12} & \bar{Q}_{22} & \bar{Q}_{26} & 0 & 0 \\ \bar{Q}_{16} & \bar{Q}_{26} & \bar{Q}_{66} & 0 & 0 \\ 0 & 0 & 0 & \bar{Q}_{55} & \bar{Q}_{45} \\ 0 & 0 & 0 & \bar{Q}_{45} & \bar{Q}_{44} \end{bmatrix}^{(k)} \begin{Bmatrix} \varepsilon_{xx} \\ \varepsilon_{yy} \\ \gamma_{xy} \\ \gamma_{xz} \\ \gamma_{yz} \end{Bmatrix}^{(k)}, \tag{4}$$

where $\bar{Q}_{ij}$ are the elastic constants of the kth layer with respect to the global Cartesian axes and their detailed definitions can be found in [1].

3. Derivation of flexure laminated plate equations

Considering the static version of the principle of virtual work, the following expressions can be obtained:

$$\begin{aligned} 0 = \int_R \Bigg\{ \int_{-h/2}^{h/2} \Big[&\sigma_{xx}^{(k)}\delta\varepsilon_{xx} + \sigma_{yy}^{(k)}\delta\varepsilon_{yy} + \tau_{xy}^{(k)}\delta\gamma_{xy} + \tau_{xz}^{(k)}\delta\gamma_{xz} \\ &+\tau_{yz}^{(k)}\delta\gamma_{yz}\Big] dz \Bigg\} dxdy - \int_R q\delta w dxdy, \end{aligned} \tag{5}$$

where q is the distributed transverse load and R is the midplane plate domain in the (x, y) Cartesian coordinates.

Substituting the virtual strains obtained from Eq. (2) and integrating along z axis, the following expression in matrix form is found:

$$\begin{aligned} 0 = &\int_R (\delta\boldsymbol{\varepsilon}_s^T\mathbf{A}\boldsymbol{\varepsilon}_s + \delta\boldsymbol{\varepsilon}_\kappa^T\mathbf{D}\boldsymbol{\varepsilon}_\kappa - \delta\boldsymbol{\varepsilon}_\kappa^T\mathbf{H}\boldsymbol{\varepsilon}_s - \delta\boldsymbol{\varepsilon}_s^T\mathbf{H}\boldsymbol{\varepsilon}_\kappa + \delta\boldsymbol{\varphi}^T\mathbf{A}^S\boldsymbol{\varphi})dxdy \\ &- \int_R q(x, y)\delta w dxdy, \end{aligned} \tag{6}$$

where

$$\mathbf{A} = \begin{bmatrix} A_{11} & A_{12} & A_{16} \\ A_{12} & A_{22} & A_{26} \\ A_{16} & A_{26} & A_{66} \end{bmatrix} \mathbf{H} = \begin{bmatrix} H_{11} & H_{12} & H_{16} \\ H_{12} & H_{22} & H_{26} \\ H_{16} & H_{26} & H_{66} \end{bmatrix}$$
$$\mathbf{D} = \begin{bmatrix} D_{11} & D_{12} & D_{16} \\ D_{12} & D_{22} & D_{26} \\ D_{16} & D_{26} & D_{66} \end{bmatrix} \mathbf{A}^S = \begin{bmatrix} A_{44}^S & A_{45}^S \\ A_{45}^S & A_{55}^S, \end{bmatrix} \tag{7}$$

being:

$$A_{ij} = \int_{-h/2}^{h/2} \overline{Q}_{ij} \sin^2\left(\frac{\pi z}{h}\right) dz, \quad A_{ij}^S = \left(\frac{\pi}{h}\right)^2 \int_{-h/2}^{h/2} \overline{Q}_{ij} \cos^2\left(\frac{\pi z}{h}\right) dz,$$

$$H_{ij} = \int_{-h/2}^{h/2} \overline{Q}_{ij} z \sin\left(\frac{\pi z}{h}\right) dz, \quad D_{ij} = \int_{-h/2}^{h/2} \overline{Q}_{ij} z^2 dz, \tag{8}$$

4. Macro finite element formulation

Due to complexity of the laminated plate geometry and the presence of couplings in the governing equations, it is extremely difficult, if not impossible, to obtain closed form solutions of the corresponding equations, particularly under arbitrary boundary conditions. Hence, approximated methods should be employed to solve the problem. In this work a macro finite element is formulated for the global static behavior analysis of laminated plates. This methodology follows the general approach of reference [22] and it has been shown that it has a simple formulation, low computational cost, and good accuracy. In addition, the macro element is free of shear locking phenomenon that occurs in the conventional finite element method.

To obtain the macro finite element, first the material points of the quadrilateral plates in the physical domain (Cartesian coordinates) are transformed into the computational domain (natural coordinates) as shown in Figure 1. The mapping process follows the standard procedure [24], i.e.:

$$x = \sum_{i=1}^{4} M_i(\xi, \eta) x_i, \qquad y = \sum_{i=1}^{4} M_i(\xi, \eta) y_i, \tag{9}$$

where (x_i, y_i), $i = 1, \ldots, 4$ are the coordinates of the four corners of the quadrilateral region R and $M_i(\xi, \eta)$ are the interpolation functions of the serendipity family [24].

The macro finite element equations are obtained by means of a hierarchical version of FEM [22, 25–27]. The convergence in the h-p version of FEM is sought by simultaneously refining the mesh and increasing the degree of the elements. As it has been demonstrated by the authors in previous works [22, 27], a very good convergence can be obtained increasing the amount of hierarchy Gram-Schmidt orthogonal polynomials and using a single quadrilateral element.

The unknown functions w, ϕ_x, ϕ_y in Eq. (1) are approximated by the product of the shape functions in the natural coordinates (ξ, η), by the respective generalized displacements:

$$\begin{aligned}
w(\xi,\eta) &= \sum_{i,j=1}^{n} p_i^{(w)}(\xi)\, q_j^{(w)}(\eta)\, c_{ij}^{(w)} = \{N^{(w)}\}\{c^{(w)}\},\\
\phi_x(\xi,\eta) &= \sum_{i,j=1}^{m} p_i^{(\phi)}(\xi)\, q_j^{(\phi)}(\eta)\, c_{ij}^{(\phi_x)} = \{N^{(\phi)}\}\{c^{(\phi_x)}\},\\
\phi_y(\xi,\eta) &= \sum_{i,j=1}^{m} p_i^{(\phi)}(\xi)\, q_j^{(\phi)}(\eta)\, c_{ij}^{(\phi_y)} = \{N^{(\phi)}\}\{c^{(\phi_y)}\}.
\end{aligned} \tag{10}$$

The first polynomials in $\{N^{(\bullet)}\} = \mathbf{N}^{(\bullet)}$, $(\bullet) = w, \phi$ are the Hermite cubic polynomials for $p_i{}^{(w)}(\xi)$, $q_j{}^{(w)}(\eta)$ $(i, j = 1 \ldots 4)$, and Hermite linear polynomials for $p_i{}^{(\phi)}(\xi)$, $q_j{}^{(\phi)}(\eta)$ $(i, j = 1, 2)$. Then, an adequate number of Gram-Schmidt polynomials are added to formulate a polynomially-enriched plate macro element: $p_i{}^{(w)}(\xi)$, $q_j{}^{(w)}(\eta)$ $(i, j = 5 \ldots n)$ and $p_i{}^{(\phi)}(\xi)$, $q_j{}^{(\phi)}(\eta)$ $(i, j = 3 \ldots m)$. The degree of the first Gram-Schmidt polynomial in both natural coordinates is four (4) for the transversal displacement w and two (2) for the rotations ϕ_x, ϕ_y. The members of the set of characteristic orthogonal polynomials are obtained following the procedure described in [27–29] as briefly described in Appendix A.

This way, the hierarchical modes contribute only to the internal displacement of the element, and do not therefore affect the displacement along the element edges or at the element nodes. Nevertheless, products obtained between any of the Gram-Schmidt (GS) characteristics orthogonal polynomials and the Hermite polynomials will constitute what amounts to edge freedoms along the element boundaries.

Replacing the expressions of Eq. (9) in conjunction with the chain rules to change the first- and second-order derivatives given in Appendix B, and the approximating functions [Eq. (10)] into the virtual work formulation [Eq. (6)], the following equation system is obtained:

$$\begin{aligned}
\mathbf{0} = \int_{-1}^{1}\int_{-1}^{1} \Big(&\delta\mathbf{c}^T\mathbf{B}^{(1)}\mathbf{A}\mathbf{B}^{(1)^T}\mathbf{c} + \delta\mathbf{c}^T\mathbf{B}^{(2)}\mathbf{D}\mathbf{B}^{(2)^T}\mathbf{c} - \delta\mathbf{c}^T\mathbf{B}^{(2)}\mathbf{H}\mathbf{B}^{(1)^T}\mathbf{c}\\
&-\delta\mathbf{c}^T\mathbf{B}^{(1)}\mathbf{H}\mathbf{B}^{(2)^T}\mathbf{c} + \delta\mathbf{c}^T\mathbf{B}^{(3)}\mathbf{A}^S\mathbf{B}^{(3)^T}\mathbf{c} - \delta\mathbf{c}^T\mathbf{B}^{(4)}q\Big)\,|\mathbf{J}|\,d\xi\,d\eta
\end{aligned} \tag{11}$$

where

$$\mathbf{B}^{(1)} = \begin{bmatrix} 0 & 0 & 0 \\ \mathbf{A1} & 0 & \mathbf{A2} \\ 0 & \mathbf{A2} & \mathbf{A1} \end{bmatrix}; \quad \mathbf{B}^{(2)} = \begin{bmatrix} \mathbf{A3} & \mathbf{A4} & 2\mathbf{A5} \\ 0 & 0 & 0 \\ 0 & 0 & 0 \end{bmatrix};$$
$$\mathbf{B}^{(3)} = \begin{bmatrix} 0 & 0 \\ 0 & \mathbf{N}^{(\phi)} \\ \mathbf{N}^{(\phi)} & 0 \end{bmatrix}; \quad \mathbf{B}^{(4)} = \begin{bmatrix} \mathbf{N}^{(w)} \\ 0 \\ 0 \end{bmatrix} \tag{12}$$

with

$$\begin{aligned}
\mathbf{A1} &= \frac{J_{22}}{|\mathbf{J}|}\frac{\partial \mathbf{N}^{(\phi)}}{\partial \xi} - \frac{J_{12}}{|\mathbf{J}|}\frac{\partial \mathbf{N}^{(\phi)}}{\partial \eta}, \qquad \mathbf{A2} = -\frac{J_{21}}{|\mathbf{J}|}\frac{\partial \mathbf{N}^{(\phi)}}{\partial \xi} + \frac{J_{11}}{|\mathbf{J}|}\frac{\partial \mathbf{N}^{(\phi)}}{\partial \eta}\\
\mathbf{A3} &= a_1'\frac{\partial^2 \mathbf{N}^{(w)}}{\partial \xi^2} + a_2'\frac{\partial^2 \mathbf{N}^{(w)}}{\partial \eta^2} - a_3'\frac{\partial^2 \mathbf{N}^{(w)}}{\partial \xi\,\partial \eta}\\
&\quad + \sum_{i=1}^{3} a_i'\left(\alpha_i'\frac{\partial \mathbf{N}^{(w)}}{\partial \xi} + \beta_i'\frac{\partial \mathbf{N}^{(w)}}{\partial \eta}\right)\\
\mathbf{A4} &= b_1'\frac{\partial^2 \mathbf{N}^{(w)}}{\partial \xi^2} + b_2'\frac{\partial^2 \mathbf{N}^{(w)}}{\partial \eta^2} - b_3'\frac{\partial^2 \mathbf{N}^{(w)}}{\partial \xi\,\partial \eta}\\
&\quad + \sum_{i=1}^{3} b_i'\left(\alpha_i'\frac{\partial \mathbf{N}^{(w)}}{\partial \xi} + \beta_i'\frac{\partial \mathbf{N}^{(w)}}{\partial \eta}\right)\\
\mathbf{A5} &= -c_1'\frac{\partial^2 \mathbf{N}^{(w)}}{\partial \xi^2} - c_2'\frac{\partial^2 \mathbf{N}^{(w)}}{\partial \eta^2} + c_3'\frac{\partial^2 \mathbf{N}^{(w)}}{\partial \xi\,\partial \eta}\\
&\quad - \sum_{i=1}^{3} c_i'\left(\alpha_i'\frac{\partial \mathbf{N}^{(w)}}{\partial \xi} + \beta_i'\frac{\partial \mathbf{N}^{(w)}}{\partial \eta}\right),
\end{aligned} \tag{13}$$

Finally, for arbitrary values of virtual displacements, Eq. (11) reduces to:

$$\mathbf{K}\mathbf{c} = \mathbf{F}, \tag{14}$$

Table 1. Square isotropic plate SSSS.

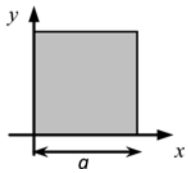

	a/h							
	10		20		50		100	
	$\overline{w}$	$\overline{\sigma}_{xx}$	$\overline{w}$	$\overline{\sigma}_{xx}$	$\overline{w}$	$\overline{\sigma}_{xx}$	$\overline{w}$	$\overline{\sigma}_{xx}$
Exact analytical solution Reddy [6]	4.7910	0.2762	4.6250	0.2762	4.5790	0.2762	4.5720	0.2762
Ferreira et al. [11]	4.7883	0.2779	4.6158	0.2765	4.5781	0.2763	4.5715	0.2762
Present TSDT $m = 4$	4.7910	0.2762	4.6250	0.2762	4.5790	0.2762	4.5720	0.2762

where $\mathbf{c}$ is the unknown displacement vector given by:

$$\mathbf{c} = \left\{ \mathbf{c}^{(w)^T} \; \mathbf{c}^{(\phi_x)^T} \; \mathbf{c}^{(\phi_y)^T} \right\} \tag{15}$$

The stiffness matrix $\mathbf{K}$ and the load vector $\mathbf{F}$ are respectively given by:

$$\mathbf{K} = \int_{-1}^{1}\int_{-1}^{1} \Big(\mathbf{B}^{(1)}\mathbf{A}\mathbf{B}^{(1)^T} + \mathbf{B}^{(2)}\mathbf{D}\mathbf{B}^{(2)^T} - \mathbf{B}^{(2)}\mathbf{H}\mathbf{B}^{(1)^T} - \mathbf{B}^{(1)}\mathbf{H}\mathbf{B}^{(2)^T} + \mathbf{B}^{(3)}\mathbf{A}^S\mathbf{B}^{(3)^T} \Big) |\mathbf{J}| \, d\xi \, d\eta \tag{16}$$

$$\mathbf{F} = \int_{-1}^{1}\int_{-1}^{1} q\mathbf{B}^{(4)} \; |\mathbf{J}| \, d\xi \, d\eta \tag{17}$$

Different boundary conditions may be applied to the laminated plate, removing from the stiffness matrix $\mathbf{K}$ and load vector $\mathbf{F}$ the rows and columns that correspond to the degrees of freedom associated with the corresponding support conditions.

5. Numerical results and discussion

The macro finite element solutions of quadrilateral laminated plates under uniform distributed load q obtained by a TSDT are presented in this section. The model developed herein is validated by comparing the results with other available solutions. For describing the boundary conditions of the plates analyzed, the following designation is employed: C for a clamped edge and S for a simply supported edge.

5.1. *Square isotropic and laminated plates*

The first example corresponds to a simply supported square isotropic plate (side length a and thickness h) with Poisson's ratio $\nu = 0.3$. The normalized transverse displacement $\bar{w}$ and normal x-stress $\bar{\sigma}_{xx}$ are obtained as:

$$\bar{w} = \frac{100Eh^3}{qa^4} w\left(\tfrac{a}{2}, \tfrac{a}{2}, 0\right), \quad \bar{\sigma}_{xx} = \frac{h^2}{qa^2}\sigma_{xx}\left(\tfrac{a}{2}, \tfrac{a}{2}, \tfrac{h}{2}\right).$$

In Table 1 the numerical results obtained with the present approach are compared with exact analytical ones from Reddy [6] and with those of Ferreira et al. [11], who used for the first time the TSDT for modeling symmetric composite plates discretized by a meshless method. It can be observed that the results

Table 2. Square laminated plate (0/90/90/0) SSSS.

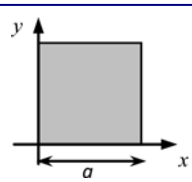

a/h		$\overline{w}$	$\overline{\sigma}_{xx}$	$\overline{\sigma}_{yy}$	$\bar{\tau}_{xy}$	$\bar{\tau}_{xz}$	$\bar{\tau}_{yz}$
20	3D-FEM [30]	0.7794	0.8207	0.4870	0.0444	0.6040	0.4738
	HSDT-MQ [30]	0.7506	0.8100	0.4775	0.0405	0.9200	0.3925
	HSDT (NS) [31]	0.7966	0.8251	0.4144	0.0469	0.6940	0.3934
	Present TSDT $m = 3$	0.7569	0.8243	0.4178	0.0422	0.5775	0.4042
	Present TSDT $m = 4$	0.7566	0.8226	0.4180	0.0425	0.5688	0.3906
	Present TSDT $m = 5$	0.7565	0.8224	0.4172	0.0428	0.5737	0.3975
10	3D-FEM [30]	1.0576	0.8201	0.5605	0.0577	0.5781	0.4980
	HSDT-MQ [30]	0.9730	0.8020	0.5380	0.0478	0.8790	0.4390
	HSDT (NS) [31]	1.1184	0.8331	0.5495	0.0615	0.6534	0.4274
	Present TSDT $m = 3$	1.0765	0.8228	0.5604	0.0540	0.5351	0.4430
	Present TSDT $m = 4$	1.0738	0.8152	0.5603	0.0538	0.5206	0.4313
	Present TSDT $m = 5$	1.0737	0.8160	0.5595	0.0548	0.5245	0.4343
5	3D-FEM [30]	2.1044	0.8995	0.7386	0.0991	0.5340	0.4487
	HSDT-MQ [30]	1.8100	0.8400	0.6600	0.0696	0.7780	0.4960
	HSDT (NS) [31]	2.1936	0.9202	0.8287	0.0900	0.5846	0.5086
	Present TSDT $m = 3$	2.1548	0.8963	0.8542	0.0848	0.4329	0.5347
	Present TSDT $m = 4$	2.1355	0.8588	0.8507	0.0802	0.4193	0.5160
	Present TSDT $m = 5$	2.1352	0.8622	0.8504	0.0842	0.4220	0.5105

Table 3. Skew laminated plate (0/90/0) SSSS.

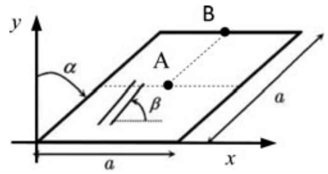

		$a/h=10$				$a/h=5$			
α	Method	$\overline{w}^A$	$\bar{\sigma}_{xx}^A$ $(z=\frac{h}{2})$	$\bar{\tau}_{yz}^B$ $(z=0)$	$\bar{\tau}_{yz}^B$ $(z=\frac{h}{6})$	$\overline{w}^A$	$\bar{\sigma}_{xx}^A$ $(z=\frac{h}{2})$	$\bar{\tau}_{yz}^B$ $(z=0)$	$\bar{\tau}_{yz}^B$ $(z=\frac{h}{6})$
30°	Chakrabarti et al. [32]	0.8814	0.7125	—	0.2145	1.6811	0.8589	—	0.2331
	Ramesh et al. [33]	0.8666	0.6934	0.4662	0.1563	1.6713	0.7909	0.4951	0.1855
	Present TSDT $m=4$	0.8441	0.6753	0.4383	0.1518	1.6346	0.7456	0.4686	0.1623
45°	Chakrabarti et al. [32]	0.5742	0.4861	—	0.2119	1.1790	0.5920	—	0.2013
	Ramesh et al. [33]	0.5745	0.4744	0.4765	0.1518	1.0980	0.5387	0.4475	0.1666
	Present TSDT $m=4$	0.5605	0.4594	0.4611	0.1597	1.0513	0.5173	0.4426	0.1533
60°	Chakrabarti et al. [32]	0.2481	0.2201	—	0.1623	0.5196	0.2906	—	0.1383
	Ramesh et al. [33]	0.2541	0.2173	0.3735	0.1195	0.5185	0.2598	0.3126	0.1265
	Present TSDT $m=4$	0.2360	0.2164	0.3435	0.1190	0.4653	0.2622	0.3010	0.1043

obtained with the present formulation are in excellent agreement with exact solutions.

The second example corresponds to a simply supported four layer 0/90/90/0 square laminated plate. The normalized displacement and stresses of the plate are defined as:

$$\bar{w} = \frac{100E_2h^3}{qa^4} w\left(\tfrac{a}{2}, \tfrac{a}{2}, 0\right), \ \bar{\sigma}_{xx} = \frac{h^2}{qa^2}\sigma_{xx}\left(\tfrac{a}{2}, \tfrac{a}{2}, \tfrac{h}{2}\right),$$
$$\bar{\sigma}_{yy} = \frac{h^2}{qa^2}\sigma_{yy}\left(\tfrac{a}{2}, \tfrac{a}{2}, \tfrac{h}{4}\right), \ \bar{\tau}_{xy} = \frac{h^2}{qa}\tau_{xy}\left(0, 0, \tfrac{h}{2}\right),$$
$$\bar{\tau}_{xz} = \frac{h}{qa}\tau_{xz}\left(0, \tfrac{a}{2}, 0\right), \ \bar{\tau}_{yz} = \frac{h}{qa}\tau_{yz}\left(\tfrac{a}{2}, 0, 0\right).$$

For this case, the material properties are $E_1/E_2 = 25$, $G_{12} = G_{13} = 0.5E_2$.

In Table 2 center point deflections and stresses are presented for three length-to-thickness ratios: $a/h = 5$, 10, 20 and for three to five polynomials of Gram-Schmidt, in order to show the convergence of results obtained with the present formulation. The present solutions are compared with results derived from the Multiquadric (MQ) function using meshless local Petrov-Galerkin solution based on HSDT and 3D-FEM solution [30] and results obtained with a numerical procedure based on node-based smoothed discrete shear gap method associated with HSDT [31]. It can be seen that all results show a good convergence and they are in very good agreement with the results published by the mentioned authors.

5.2. *Skew laminated plates*

In this section, simply supported 0/90/0 skew plates for various skew angles α and length-to-thickness ratios a/h are considered using four polynomials of Gram-Schmidt ($m = 4$). The material properties and the normalized displacement and stresses are the same of the example depicted in the previous section. The results obtained by means of the present approach are compared

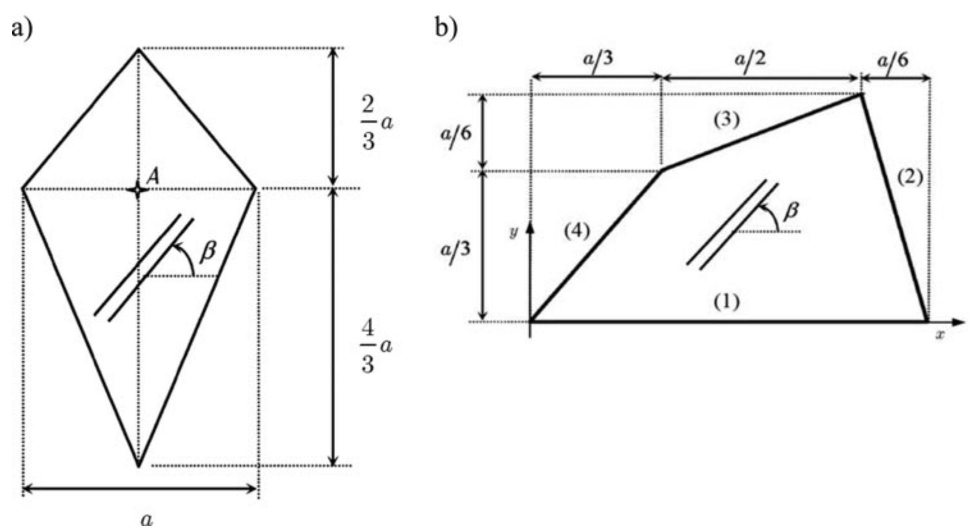

Figure 2. (a) Geometry of rhomboidal plate and (b) geometry of general quadrilateral plate.

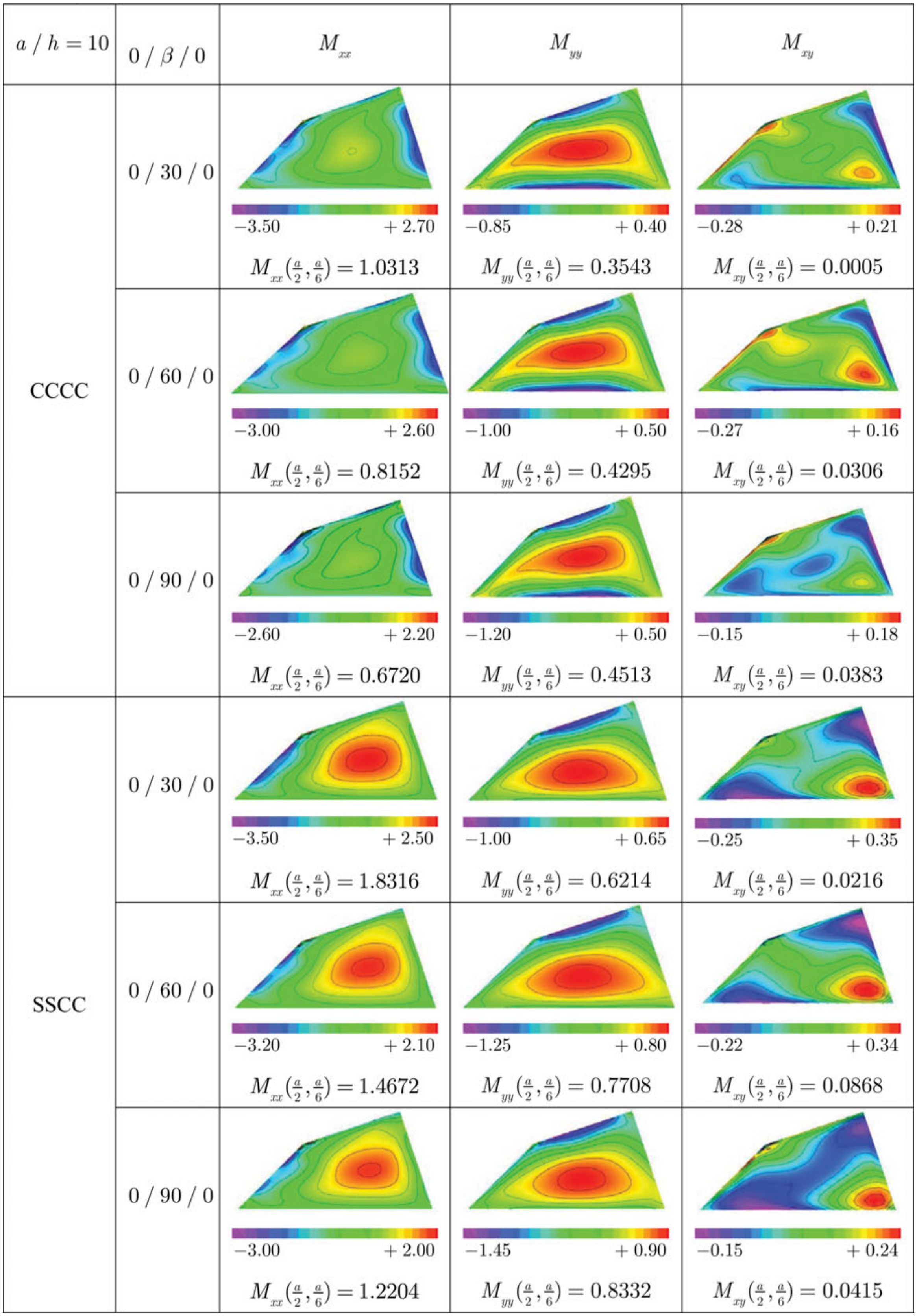

Figure 3. Contour plots of bending and twisting moments for general quadrilateral plates.

Table 4. Rhomboidal laminated plate (5.3) SSSS

	β	$a/h = 5$ $\overline{w}^A$	$a/h = 5$ $\overline{M}^A_{xx}$	$a/h = 10$ $\overline{w}^A$	$a/h = 10$ $\overline{M}^A_{xx}$	$a/h = 20$ $\overline{w}^A$	$a/h = 20$ $\overline{M}^A_{xx}$	$a/h = 100$ $\overline{w}^A$	$a/h = 100$ $\overline{M}^A_{xx}$	$a/h = 1000$ $\overline{w}^A$	$a/h = 1000$ $\overline{M}^A_{xx}$
Nallim et al. [28]	0°	—	—	—	—	—	—	—	—	4.3042	4.7543
Present TSDT $m = 4$		6.9413	4.8138	4.9777	4.7388	4.4194	4.6931	4.2248	4.6725	4.2165	4.6715
Nallim et al. [28]	15°	—	—	—	—	—	—	—	—	4.3980	4.9629
Present TSDT $m = 4$		6.3590	5.1574	4.8845	4.9939	4.4624	4.9179	4.3078	4.8848	4.3010	4.8833
Nallim et al. [28]	30°	—	—	—	—	—	—	—	—	4.8641	4.8825
Present TSDT $m = 4$		7.0847	5.0566	5.4339	4.9267	4.9621	4.8612	4.7931	4.8323	4.7858	4.8310
Nallim et al. [28]	45°	—	—	—	—	—	—	—	—	5.4583	4.5766
Present TSDT $m = 4$		7.9498	4.7744	6.1304	4.6473	5.6037	4.5798	5.4152	4.5502	5.4071	4.5489
Nallim et al. [28]	60°	—	—	—	—	—	—	—	—	5.8797	4.0422
Present TSDT $m = 4$		8.6177	4.2936	6.6593	4.1466	6.0738	4.0652	5.8592	4.0280	5.8498	4.0263
Nallim et al. [28]	75°	—	—	—	—	—	—	—	—	5.9731	3.5619
Present TSDT $m = 4$		8.9255	3.8319	6.8506	3.6790	6.2067	3.5915	5.9639	3.5502	5.9532	3.5482
Nallim et al. [28]	90°	—	—	—	—	—	—	—	—	5.5124	3.5819
Present TSDT $m = 4$		7.9531	4.0169	6.2764	3.7361	5.7237	3.6181	5.4980	3.5661	5.4876	3.5636

with those of Chakrabarti and Sheikh [32] who employed a six-noded triangular finite element with a refined HSDT and with those of Ramesh et al. [33] who used a higher-order triangular plate element based on the third-order shear deformation theory. It can be observed from Table 3 that the results obtained from the present formulation using four Gram-Schmidt polynomials are in good agreement with the solutions reported by other authors.

5.3. *Rhomboidal laminated plates*

In this section, results for rhomboidal laminates (Figure 2a) are presented. Four-ply E-glass/epoxy laminates are considered, with the following material properties:

$$E_1 = 60.7\,GPa, \quad E_2 = 24.8\,GPa, \; G_{12} = 12\,GPa,$$
$$G_{13} = 0.5E_2, \quad G_{23} = 0.2E_2, \quad \nu_{12} = 0.23$$

and with 5.3 stacking sequence. As shown in Table 4, SSSS boundary conditions and length-to-thickness ratios $a/h = 5, 10, 20, 100, 1000$ are considered. The angle of fiber orientation ranges from $\beta = 0^\circ$ to $\beta = 90^\circ$. In this table, $\beta = 0^\circ$ and $\beta = 90^\circ$ mean cross-ply laminates with stacking sequences 0/90/90/0 and 90/0/0/90, respectively. Deflections and bending moments in point A (Figure 2a) of the rhomboidal plate are normalized as:

$$\overline{w}^A = \frac{100 E_1 h^3}{q a^4} w^A, \qquad \overline{M}^A_{xx} = \frac{100}{q a^2} M^A_{xx}.$$

Particularly, the results corresponding to the case of $a/h = 1000$ are compared with those obtained by Nallim et al. [28], who studied arbitrary quadrilateral anisotropic thin plates using a formulation based on the Ritz method in conjunction with natural coordinates and CLPT. When thin plate is considered, it can be seen that the present formulation is free of shear-locking phenomenon and then results for $a/h = 1000$ approach to those obtained by CLPT.

5.4. *General quadrilateral laminated plates*

The developed formulation has been further applied to the static analysis of laminated plates with general quadrilateral planforms (Figure 2b), stacking sequence $0/\beta/0$, length-to-thickness ratio $a/h = 10$, and boundary conditions CCCC and SSCC. The terminology SSCC means that edges (1) and (2) are simply supported and edges (3) and (4) are clamped (see Figure 2b).

The assumed material properties are the same as those used in Section 5.1 as well as the normalized displacement and stresses of the plate. Table 5 lists the deflections and the stresses at different points as computed with the methodology developed in this article. Results are for three stacking sequences and for two different boundary conditions.

For each laminated plate, Figure 3 shows the contour plots of bending moments (M_{xx}, M_{yy}) and twisting moment (M_{xy}) and also includes values of normalized moments in a specific point that can be used for comparison purposes. By comparing the contour plots, the influence of fiber orientation angles and boundary conditions in the results can be observed. It can be seen that the most remarkable differences occur in twisting

Table 5. General quadrilateral laminated plate ($0/\beta/0$)

	$0/\beta/0$	$\overline{w}(\frac{a}{2}, \frac{a}{6})$	$\overline{\sigma}_{xx}(\frac{a}{2}, \frac{a}{6}, \frac{h}{2})$	$\overline{\sigma}_{yy}(\frac{a}{2}, \frac{a}{6}, \frac{h}{2})$	$\overline{\tau}_{xy}(\frac{a}{2}, \frac{a}{6}, \frac{h}{2})$	$\overline{\tau}_{xz}(\frac{a}{3}, \frac{a}{6}, 0)$	$\overline{\tau}_{yz}(\frac{a}{3}, \frac{a}{6}, 0)$
CCCC	0/30/0	0.0918	0.0761	0.0231	0.0020	0.1173	0.0229
	0/60/0	0.0833	0.0620	0.0213	0.0025	0.0667	0.0347
	0/90/0	0.0744	0.0511	0.0180	0.0025	0.0560	0.0572
SSCC	0/30/0	0.1386	0.1366	0.0373	0.0026	0.1966	0.0378
	0/60/0	0.1262	0.1131	0.0342	0.0031	0.1095	0.0636
	0/90/0	0.1117	0.0964	0.0294	0.0028	0.0951	0.1063

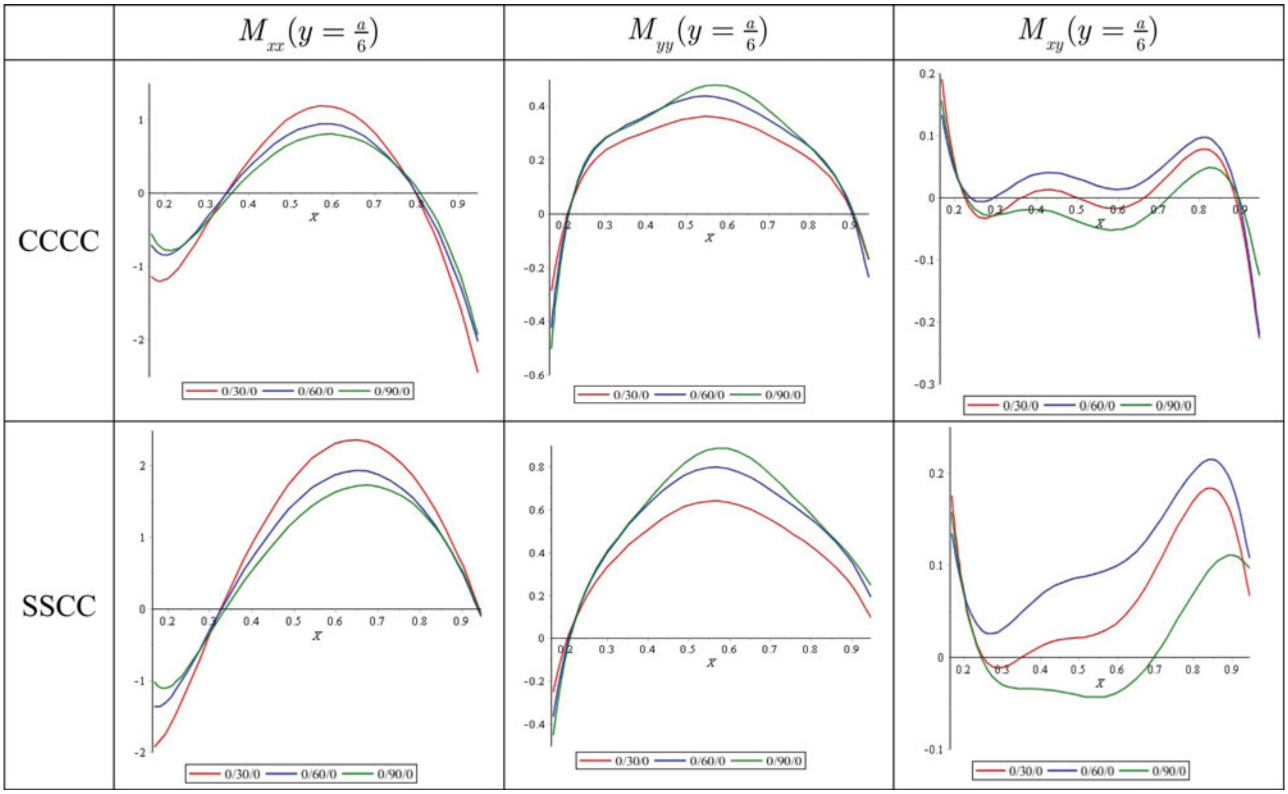

Figure 4. Variation of bending and twisting moments for general quadrilateral plates along *x*-axis.

moments. Figure 4 presents the variation of bending and twisting moments for $y = a/6$, along a line parallel to x-axis. It can be observed that for the two analyzed boundary conditions, the bending moment M_{xx} takes larger values for staking sequence 0/30/0, while for the bending moments M_{yy} and for the twisting moments M_{xy} the maximum values are obtained for stacking sequence 0/90/0 and 0/60/0, respectively.

Finally, Figures 5, 6, and 7 show the variation of normalized transverse displacement $\overline{w}$ and normalized bending moment $\bar{M}_{xx}$ of CCCC, SSCC, and SSSS general quadrilateral plates, respectively, for stacking sequence $0/\beta/0$ with different angles of fiber orientation β and a/h ratios. Once again it can be observed that this formulation is free from shear-locking phenomenon.

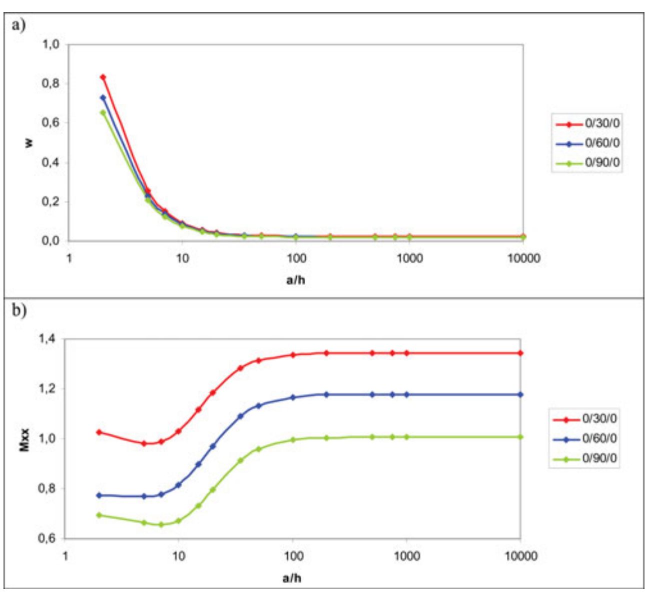

Figure 5. Effect of length-to-thickness ratio on normalized transverse displacement $\bar{w}$ (a) and normalized bending moment $\bar{M}_{xx}$ (b) of the CCCC general quadrilateral plate $0/\beta/0$ for different angles of fiber orientation β and *a*/*h* ratios.

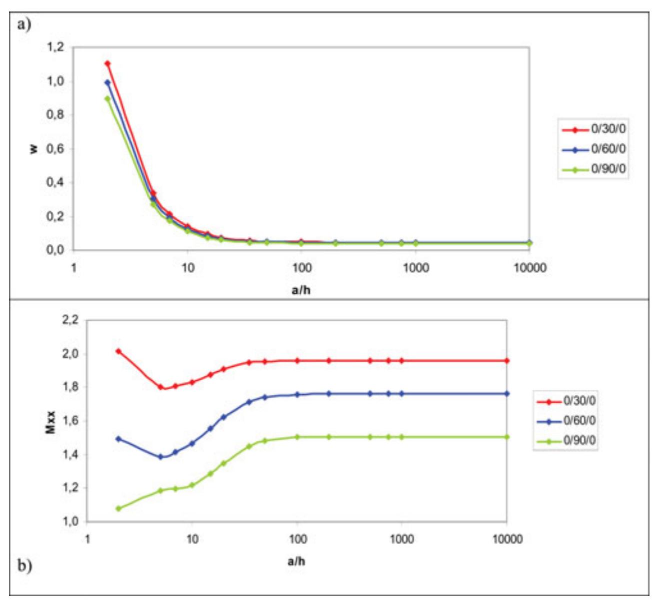

Figure 6. Effect of length-to-thickness ratio on normalized transverse displacement $\bar{w}$ (a) and normalized bending moment $\bar{M}_{xx}$ (b) of the SSCC general quadrilateral plate $0/\beta/0$ for different angles of fiber orientation β and *a*/*h* ratios.

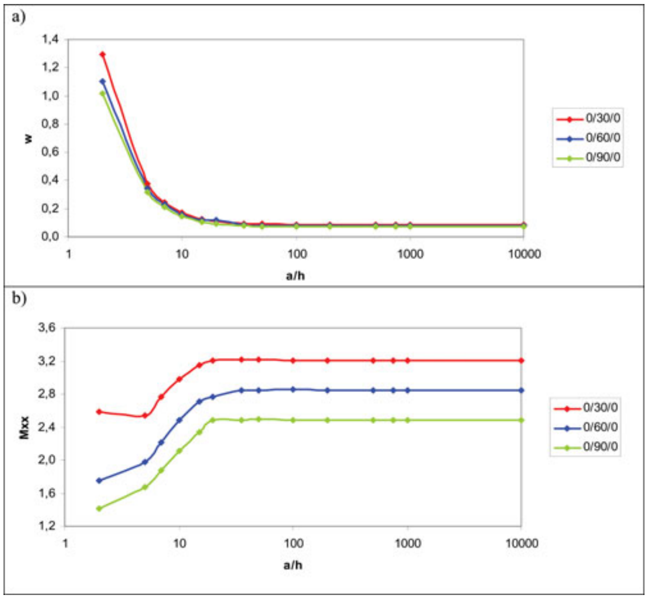

Figure 7. Effect of length-to-thickness ratio on normalized transverse displacement $\bar{w}$ (a) and normalized bending moment $\bar{M}_{xx}$ (b) of the SSSS general quadrilateral plate 0/β/0 for different angles of fiber orientation β and a/h ratios.

6. Conclusions

A hierarchical macro finite element based on the trigonometric shear deformation theory has been developed for the static analysis of general quadrilateral laminated composite plates. In the TSDT, shear stresses free boundary conditions at the top and bottom surfaces of the plates are satisfied and hence shear correction factors are ignored. A weak form of the static model for laminated composite plates based on the principle of virtual work is derived. The macro finite element is obtained considering Hermite polynomials as locally supported functions, enriched with orthogonal polynomials generated by the Gram-Schmidt procedure. The accuracy of results obtained using the present formulation is demonstrated by comparing some results to the 3D elasticity solution and those available in the literature. Obtained results show high reliability for all test cases from the thin to thick plates. The examples demonstrate the ability of enriched macro element in handling general quadrilateral geometries. Good convergence is found using Gram-Schmidt polynomials in each plane plate direction, so the present method constitutes an effective alternative for the analysis of laminated composite plates in practical applications.

In the developed formulation only symmetric laminated plates are considered, so the bending and in-plane deformations are uncoupled, and just three components of the displacement field were approximated in the presented approach (i.e., w, ϕ_x, ϕ_y). Following a similar procedure, the present method can be easily extended to consider nonsymmetric laminated plates.

Funding

The present investigation has been sponsored by the CIUNSA Project 2218. S. Oller acknowledges the financial support of the “COMP-DES-MAT” (ERC-2012-AdG 320815) research project of the European Research Council (ERC) of the European Commission.

References

[1] J.N. Reddy, Mechanics of Laminated Composite Plates and Shells—Theory and Analysis, CRC Press, Boca Raton, FL, 2004.
[2] S.G. Lekhnitskii, Anisotropic Plates, Gordon and Breach Science Publishers, New York, NY, 1968.
[3] E. Reissner, The effect of transverse shear deformation on the bending of elastic plates, J. Appl. Mech., vol. 12, no. 2, pp. 69–77, 1945.
[4] R.D. Mindlin, Influence of rotary inertia and shear on flexural motions of isotropic elastic plates, J. Appl. Mech., vol. 18, pp. 31–38, 1951.
[5] P.F. Pai, A new look at shear correction factors and warping functions of anisotropic laminates, Int. J. Solids Struct., vol. 32, no. 16, pp. 2295–2313, 1995.
[6] J.M. Reddy, A simple higher-order theory for laminated composite plates, J. Appl. Mech., vol. 51, pp. 745–752, 1984.
[7] T. Kant and K. Swaminathan, Analytical solutions for the static analysis of laminated composite and sandwich plates based on a higher order refined theory, Compos. Struct., vol. 56, pp. 329–344, 2002.
[8] J.N. Reddy and R.A. Arciniega, Shear deformation plate and shell theories: From Stavsky to present, Mech. Adv. Mater. Struct., vol. 11, no. 6, pp. 535–582, 2004.
[9] M. Karama, K.S. Afaq, and S. Mistou, A new theory for laminated composite plates, J. Mater. Des. Appl., vol. 223, no. 2, pp. 53–62, 2009.
[10] J.L. Mantari, A.S. Oktem, and C. Guedes Soares, A new higher order shear deformation theory for sandwich and composite laminated plates, Composites Part B, vol. 43, no. 3, pp. 1489–1499, 2012.
[11] A.J.M. Ferreira, C.M.C. Roque, and R.M.N. Jorge, Analysis of composite plates by trigonometric shear deformation theory and multiquadritics, Compos. Struct., vol. 83, pp. 2225–2237, 2005.
[12] S. Xiang, K. Wang, Y. Ai, Y. Sha, and H. Shi, Analysis of isotropic sandwich and laminated plates by a meshless method and various shear deformation theories, Compos. Struct., vol. 91, pp. 31–37, 2009.
[13] J.L. Mantari, A.S. Oktem, and C. Guedes Soares, A new trigonometric shear deformation theory for isotropic, laminated composite and sandwich plates, Int. J. Solids Struct., vol. 49, no. 1, pp. 43–53, 2012.
[14] Y.X. Zhang and C.H. Yang, Recent developments in finite element analysis for laminated composite plates, Compos. Struct., vol. 88, pp. 147–157, 2009.
[15] G.S. Ramtekkar, Y.M. Desai, and A.H. Shah, Mixed finite-element model for thick composite laminated plates, Mech. Adv. Mater. Struct., vol. 9, no. 2, pp. 133–156, 2002.
[16] E. Carrera, Theories and finite elements for multilayered, anisotropic, composite plates and shells, Arch. Comput. Methods Eng., vol. 9, no. 2, pp. 87–140, 2002.
[17] E. Carrera, S. Brischetto, and P. Nali, Plates and Shells for Smart Structures: Classical and Advanced Theories for Modeling and Analysis, John Wiley & Sons, West Sussex, UK, 2011.
[18] N.A. Fallah, A finite volume method for plate buckling analysis. In: III European Conference on Computational Mechanics, Springer, Netherlands, p. 690, 2006.
[19] C.M.C. Roque, D. Cunha, C. Shu, and A.J.M. Ferreira, A local radial basis functions—Finite differences technique for the analysis of composite plates, Eng. Anal. Bound. Elem., vol. 35, no. 3, pp. 363–374, 2011.
[20] G.R. Liu, Mesh Free Method: Moving Beyond the Finite Element Method, CRC Press, New York, NY, 2002.
[21] K.M. Liew, X. Zhao, and A.J.M. Ferreira, A review of meshless methods for laminated and functionally graded plates and shells, Compos. Struct., vol. 93, no. 8, pp. 2031–2041, 2011.
[22] R.F. Rango, L.G. Nallim, and S. Oller, Formulation of enriched macro elements using trigonometric shear deformation theory for free vibration analysis of symmetric laminated composite plate assemblies, Compos. Struct., vol. 119, pp. 38–49, 2015.
[23] O.C. Zienkiewicz, S.R. Gago, and D.W. Kelly, The hierarchical concept in finite element analysis, Comput. Struct., vol. 16, no. 1–4, pp. 53–65, 1983.

[24] O.C. Zienkiewicz and R.L. Taylor, The finite element method for solid and structural mechanics, Sixth Edition, Elsevier, Oxford, UK, 2005.
[25] N.S. Bardell, J.M. Dunsdon, and R.S. Langley, Free vibration analysis of thin coplanar rectangular plate assemblies—Part I: Theory and initial results for specially orthotropic plates, Compos. Struct., vol. 34, pp. 129–143, 1996.
[26] N.S. Bardell, J.M. Dunsdon, and R.S. Langley, Free vibration analysis of thin coplanar rectangular plate assemblies—Part II: Further results for generally orthotropic plates, Compos. Struct., vol. 34, pp. 145–162, 1996.
[27] R.F. Rango, L.G. Nallim, and S. Oller, Static and dynamic analysis of thick laminated plates using enriched macroelements, Compos. Struct., vol. 101, pp. 94–103, 2013.
[28] L.G. Nallim, S. Oller, and R.O. Grossi, Statical and dynamical behaviour of thin fibre reinforced composite laminates with different shapes, Comput. Methods Appl. Mech. Eng., vol. 194, pp. 1797–1822, 2005.
[29] L.G. Nallim and S. Oller, An analytical-numerical approach to simulate the dynamic behaviour of arbitrarily laminated composite plate, Compos. Struct., vol. 85, pp. 311–325, 2008.
[30] J.R. Xiao, D.F. Gilhooley, R.C. Batra, J.W. Gillespie, and M.A. McCarthy, Analysis of thick composite laminates using a higher-order shear and normal deformable plate theory (HOSNDPT) and a meshless method, Composites Part B, vol. 39, pp. 414–427, 2008.
[31] C.H. Thai, L.V. Tran, D.T, Tran, T. Nguyen-Thoi, and H. Nguyen-Xuan, Analysis of laminated composite plates using higher-order shear deformation plate theory and node-based smoothed discrete shear gap method, Appl. Math. Modell., vol. 36, pp. 5657–5677, 2012.
[32] A. Chakrabarti and H. Sheikh, A new triangular element to model inter-laminar shear stress continuous plate theory, Int. J. Numer. Methods Eng., vol. 60, pp. 1237–1257, 2004.
[33] S.S. Ramesh, C.M. Wang, J.N. Reddy, and K.K. Ang, A higher-order plate element for accurate prediction of interlaminar stresses in laminated composite plates, Compos. Struct., vol. 91, pp. 337–357, 2009.

Appendix A

The first Gram-Schmidt polynomials in ξ natural coordinate, for w and ϕ are given by:

$$p_1^{(w)}(\xi) = 1 - 2\xi^2 + \xi^4, \quad p_1^{(\phi)}(\xi) = -1 + \xi^2.$$

The higher members are constructed by employing the Gram-Schmidt orthogonalization procedure:

$$p_2^{(\bullet)}(\xi) = \left(\xi - B_2^{(\bullet)}\right) p_1^{(\bullet)}(\xi),$$
$$p_k^{(\bullet)}(\xi) = \left(\xi - B_k^{(\bullet)}\right) p_{k-1}^{(\bullet)}(\xi) - C_k^{(\bullet)} p_{k-2}^{(\bullet)}(\xi) \qquad (\bullet) = w, \phi,$$

where

$$B_k^{(\bullet)} = \frac{\int_{-1}^{1} \xi \left(p_{k-1}^{(\bullet)}(\xi)\right)^2 d\xi}{\int_{-1}^{1} \left(p_{k-1}^{(\bullet)}(\xi)\right)^2 d\xi}, \quad C_k^{(\bullet)} = \frac{\int_{-1}^{1} \xi\, p_{k-1}^{(\bullet)}(\xi)\, p_{k-2}^{(\bullet)}(\xi)\, d\xi}{\int_{-1}^{1} \left(p_{k-2}^{(\bullet)}(\xi)\right)^2 d\xi}.$$

The coefficients of the polynomials are chosen in such a way as to make the polynomials orthonormal, $\int_{-1}^{1} (p_k^{(\bullet)}(\xi))^2 = 1$. The polynomials along the η direction are also generated using the same procedure.

Appendix B

The transformation equation (9) maps a point (ξ, η) in the master plate onto a point (x, y) in the real plate domain and vice versa if the Jacobian determinant of the transformation is given by:

$$|\mathbf{J}| = \frac{\partial x}{\partial \xi}\frac{\partial y}{\partial \eta} - \frac{\partial x}{\partial \eta}\frac{\partial y}{\partial \xi},$$

is positive.

Applying the chain rule of differentiation it can be shown that the first derivatives of a function in both spaces are related by:

$$\begin{bmatrix} \frac{\partial}{\partial x} \\ \frac{\partial}{\partial y} \end{bmatrix} = \mathbf{J}^{-1} \begin{bmatrix} \frac{\partial}{\partial \xi} \\ \frac{\partial}{\partial \eta} \end{bmatrix} = \begin{bmatrix} \frac{J_{22}}{|\mathbf{J}|} & -\frac{J_{12}}{|\mathbf{J}|} \\ -\frac{J_{21}}{|\mathbf{J}|} & \frac{J_{11}}{|\mathbf{J}|} \end{bmatrix} \begin{bmatrix} \frac{\partial}{\partial \xi} \\ \frac{\partial}{\partial \eta} \end{bmatrix}$$

where $\mathbf{J}$ is the Jacobian given by:

$$\mathbf{J} = \begin{bmatrix} J_{11} & J_{12} \\ J_{21} & J_{22} \end{bmatrix} = \begin{bmatrix} \sum x_i M_{i,\xi} & \sum y_i M_{i,\xi} \\ \sum x_i M_{i,\eta} & \sum y_i M_{i,\eta} \end{bmatrix}.$$

The elemental area $dxdy$ in the Cartesian domain R is transformed into $|\mathbf{J}|d\xi d\eta$.

Applying again the chain rule of differentiation in Eq. (14), results in:

$$\begin{bmatrix} \frac{\partial^2 w}{\partial x^2} \\ \frac{\partial^2 w}{\partial y^2} \\ \frac{\partial^2 w}{\partial x \partial y} \end{bmatrix} = \left[Op^{(1)}\right] \begin{bmatrix} \frac{\partial^2 w}{\partial \xi^2} \\ \frac{\partial^2 w}{\partial \eta^2} \\ \frac{\partial^2 w}{\partial \xi \partial \eta} \end{bmatrix} + \left[Op^{(2)}\right] \begin{bmatrix} \frac{\partial w}{\partial \xi} \\ \frac{\partial w}{\partial \eta} \end{bmatrix}$$

where the elements of the matrices $[Op^{(1)}]$ and $[Op^{(2)}]$ are given by:

$$\left[Op^{(1)}\right] = \begin{bmatrix} a_1' & a_2' & -a_3' \\ b_1' & b_2' & -b_3' \\ -c_1' & -c_2' & c_3' \end{bmatrix}$$

$$\left[Op^{(2)}\right] = \begin{bmatrix} \sum_{i=1}^{3} a_i'\alpha_i' & \sum_{i=1}^{3} a_i'\beta_i' \\ \sum_{i=1}^{3} b_i'\alpha_i' & \sum_{i=1}^{3} b_i'\beta_i' \\ -\sum_{i=1}^{3} c_i'\alpha_i' & -\sum_{i=1}^{3} c_i'\beta_i' \end{bmatrix}$$

where

$$a_1' = \frac{J_{22}^2}{|\mathbf{J}|^2}, \quad a_2' = \frac{J_{12}^2}{|\mathbf{J}|^2}, \quad a_3' = 2\frac{J_{12}J_{22}}{|\mathbf{J}|^2}$$

$$b_1' = \frac{J_{21}^2}{|\mathbf{J}|^2}, \quad b_2' = \frac{J_{11}^2}{|\mathbf{J}|^2}, \quad b_3' = 2\frac{J_{11}J_{21}}{|\mathbf{J}|^2}$$

$$c_1' = \frac{J_{21}J_{22}}{|\mathbf{J}|^2}, \quad c_2' = \frac{J_{11}J_{12}}{|\mathbf{J}|^2}, \quad c_3' = \frac{J_{11}J_{22} + J_{12}J_{21}}{|\mathbf{J}|^2}$$

$$\alpha_1' = \frac{-J_{11,\xi}J_{22} + J_{12,\xi}J_{21}}{|\mathbf{J}|} \quad \alpha_2' = \frac{-J_{21,\eta}J_{22} + J_{22,\eta}J_{21}}{|\mathbf{J}|},$$

$$\alpha_3' = \frac{J_{11,\eta}J_{22} - J_{22,\xi}J_{21}}{|\mathbf{J}|}$$

$$\beta_1' = \frac{J_{11,\xi}J_{12} - J_{12,\xi}J_{11}}{|\mathbf{J}|}, \quad \beta_2' = \frac{J_{21,\eta}J_{12} - J_{22,\eta}J_{11}}{|\mathbf{J}|},$$

$$\beta_3' = \frac{-J_{11,\eta}J_{12} + J_{22,\xi}J_{11}}{|\mathbf{J}|}$$